Research Square

Preprints are preliminary reports that have not undergone peer review.
They should not be considered conclusive, used to inform clinical practice,
or referenced by the media as validated information.

Spectral Doughnut: A Metasurface-Enabled Snapshot Hyperspectral Imager for Unresolved Resident Space Objects

Lukas Senczyszyn

lukas.senczyszyn@sdl.usu.edu

Utah State University Space Dynamics Laboratory

Christian Conkle

Utah State University Space Dynamics Laboratory

Keith Blonquist

Utah State University Space Dynamics Laboratory

Phil Scott

Utah State University Space Dynamics Laboratory

Cody Shaw

Utah State University Space Dynamics Laboratory

Zachary Coppens

CFD Research Corporation (United States)

Arturo Jiminez

CFD Research Corporation (United States)

Ronald Driggers

University of Arizona

Research Article

Keywords: metasurface optics, hyperspectral imaging, point-spread-function engineering, resident space objects, space domain awareness, SWIR, snapshot spectroscopy

Posted Date: July 28th, 2026

DOI: https://doi.org/10.21203/rs.3.rs-10035035/v1

License: This work is licensed under a Creative Commons Attribution 4.0 International License.
Read Full License

Additional Declarations: No competing interests reported.

Spectral Doughnut: A Metasurface-Enabled Snapshot Hyperspectral Imager for Unresolved Resident Space Objects

Lukas Senczyszyn[1], Christian Conkle[1], Keith Blonquist[1], Phil Scott[1], Cody Shaw[1], Zachary Coppens[2], and Arturo Jiminez[2] , and Ronald Driggers[3]

[1] Space Dynamics Laboratory, Utah State University Research Foundation, North Logan, UT, USA

[2]CFD Research Corporation, Huntsville, AL, USA

[3]University of Arizona, Tucson, AZ, USA

Correspondence: Lukas.Senczyszyn@sdl.usu.edu

ORCID (Corresponding Author): 0009-0003-1370-404X

Abstract

Space domain awareness requires optical instruments that can detect, track, and characterize resident space objects even when the targets remain unresolved by the telescope aperture. Conventional hyperspectral imagers can supply material and illumination information, but slit, grating, filter-wheel, and scanning architectures often impose size, weight, power, cost, field-of-view, cadence, and data-volume penalties that are poorly matched to rapid cueing of sparse point-source scenes. This manuscript describes Spectral Doughnut, a metasurface-based concept that maps wavelength onto the azimuthal coordinate of a chiral point-spread function. The resulting ring-shaped response preserves the source centroid for astrometry while distributing the spectral content around the source rather than along a single linear dispersion axis. The approach is intended to reduce spectral mixing among closely spaced unresolved objects and to enable snapshot spectral measurements in a compact payload. The current SWIR proof-of-concept design targets 1.1-1.7 μm operation and has a modeled spectral resolution of 38.213 nm, corresponding to approximately 15.7 resolvable samples across the band and a resolving power near 37 at 1.4 μm. We summarize the metasurface design, the integration path for an f/8 Ritchey-Chretien telescope demonstrator, the benchtop calibration sequence using a monochromator and cooled InGaAs focal plane, and the data-reduction method that converts calibrated ring angle to wavelength. The paper also identifies the principal limitations of the present on-axis demonstrator and the required future work for a pupil-conjugate, full-field implementation.

Keywords: metasurface optics; hyperspectral imaging; point-spread-function engineering; resident space objects; space domain awareness; SWIR; snapshot spectroscopy

1 Introduction

The ability to characterize resident space objects (RSOs) without spatially resolving them is a central problem in space domain awareness. Object type, material composition, attitude state, illumination geometry, and operational changes are often inferred from integrated brightness or spectral signatures rather than resolved imagery. Light curves are valuable for cadence and sensitivity, but intensity-only measurements can be ambiguous when shape, attitude, material aging, glints, range, and atmospheric transmission change simultaneously. Spectral measurements provide additional observables because reflected and emitted radiance contains information about surface materials and thermal state. For this reason, hyperspectral and multispectral techniques have been studied for material identification, object classification, and attitude reconstruction in non-resolved space object applications [1-3].

The instrument-level challenge is that many spectroscopic architectures are not naturally matched to sparse, wide-field, unresolved point-source scenes. Slit spectrometers provide clean spectra but discard most of the

field unless the target is accurately placed on the slit. Scanning systems and filter wheels can increase spectral coverage but trade against cadence and introduce moving parts. Slitless spectrometers preserve field coverage and can be compact, yet conventional gratings disperse each point source axially. When two sources have small angular separation along the dispersion axis, their spectra overlap and the spatial and spectral information become convolved. A second measurement at a different roll angle, additional optical channels, or computational deblending may be required, increasing operational complexity.

Spectral Doughnut addresses this point-source problem by replacing one-dimensional spectral dispersion with a wavelength-dependent chiral point-spread function (PSF). In the idealized geometry, each unresolved source produces a ring centered on the source location. Wavelength is encoded primarily by azimuthal angle, while the centroid of the ring encodes object position. When sources are close, ring intersections are localized rather than spread along the full spectral trace. The technique is not intended to replace high-resolution slit or echelle spectrographs. Instead, it is intended for moderate-resolution, low-SWaP-C spectral sensing where rapid cueing, field coverage, and reduced spectral mixing are more important than very high resolving power.

This paper presents the Spectral Doughnut concept as an engineering architecture for sparse point-source spectral sensing. It distinguishes the intended full-field architecture from the current Phase 1 proof-of-concept hardware, which places the metasurface in a converging f/8 telescope beam for on-axis validation. That distinction is important: the on-axis demonstrator can validate fabrication, calibration, spectral extraction, and on-sky feasibility, while a future pupil-conjugate implementation is required to realize the full-field performance implied by the concept. This full performance implementation may require a dedicated optical system rather than slotting into the filter wheel minimizing the SWaP-C advantage of the current concept in order to maximize the full-field snapshot performance for best characterizing CSOs in view.

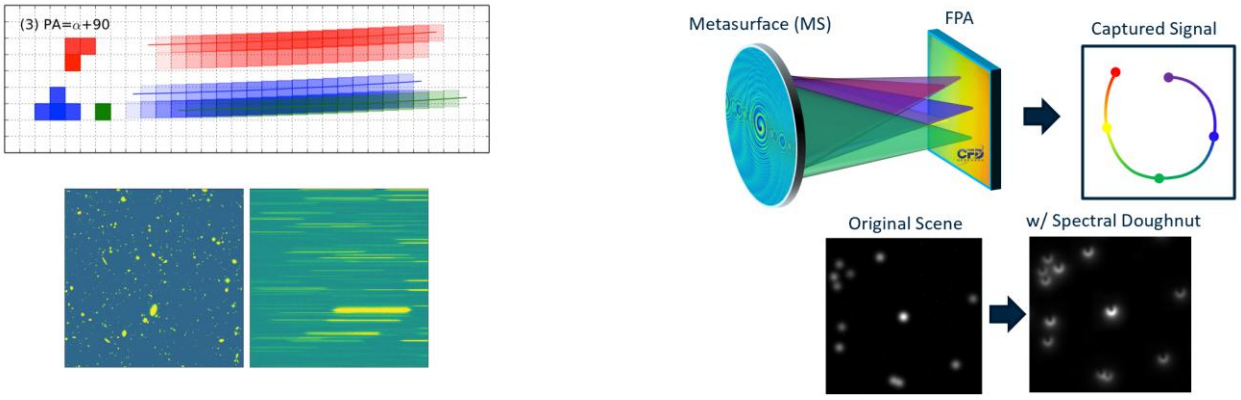


Figure 1. Conceptual comparison of axial slitless dispersion and the Spectral Doughnut response [13-14]

Table 1 Nomenclature and abbreviations.

Acronym	Definition
RSO	Resident space object, including active spacecraft, inactive satellites, rocket bodies, and orbital debris
SDA/SSA	Space domain awareness/space situational awareness; the broader detection, tracking, identification, and characterization problem
HSI	Hyperspectral imaging; here used for spectral measurements of unresolved point sources rather than a conventional spatial-spectral cube over extended scenes

PSF	Point-spread function
FPA	Focal-plane array
NUC	Nonuniformity correction
R	Resolving power, $R = \lambda/\Delta\lambda$

2 Motivation and Relationship to Existing Spectrometers

For a diffraction grating, the principal maxima are governed by the grating equation - 1) **$m\lambda = d[\sin(\alpha) + \sin(\beta)]$** here m is diffraction order, λ is wavelength, d is groove spacing, α is the incident angle, and β is the diffracted angle [4]. This relationship is the basis for compact spectrometers and slitless spectral imaging, but it also creates a geometrical trade: wavelength is mapped along a dispersion axis that is independent of scene structure. In sparse astronomical scenes, every star, RSO, or glint produces a spectral trace that may overlap.

$$\textbf{1)}\ m\lambda = d[\sin(\alpha) + \sin(\beta)]$$

Traditional wide-field slitless spectroscopy is highly useful for survey astronomy and instrument simplicity [13-14], and the Spectral Doughnut architecture should be viewed as complementary rather than as a universal replacement. The innovation is the decision to curl the spectral coordinate around each point source. A ring occupies more local area than a diffraction-limited star image, but it avoids the linear trace that can overlap a neighboring source over many spectral channels. For source separations larger than the ring diameter, spectra are separated.

The application space is therefore different from that of high resolving power instruments. The Phase 1 SWIR design has Δλ approximately 38 nm over a 1.1-1.7 μm band. At the 1.4 μm band center this corresponds to R of approximately 37. This is intended for broad material-class cues, color-temperature estimation, and star/not-star discrimination concepts [1 & 3], but it is not a substitute for high-dispersion spectroscopy. The value proposition is an inexpensive, passive, small-aperture insert that can augment an existing telescope with snapshot spectral sensitivity.

3 Metasurface and Spectral Doughnut Principle

A metasurface controls an incident wavefront with subwavelength structures, often called unit cells or meta-atoms. Each unit cell can be tuned by material, height, lateral dimensions, shape, and period. By choosing a spatial distribution of these cells, the surface imparts a designed phase and amplitude response to the transmitted or reflected field. Recent computational imaging literature has demonstrated that metasurfaces can provide compact wavelength-dependent optical encoding for hyperspectral and other high-dimensional imaging tasks [5-7].

The Spectral Doughnut design uses a chirally varying metasurface pattern to engineer a wavelength-dependent PSF. Conceptually, the metasurface assigns different phase response around the azimuthal coordinate. A point source at infinity is focused by the telescope and then modified by the metasurface so that the focal-plane irradiance forms an annulus. The angular location of the dominant energy on the annulus changes with wavelength. This converts spectral reconstruction from a mapping of a linear trace into a polar-coordinate extraction problem around each detected source centroid.

The source position is estimated from the ring centroid or from a fitted PSF model. After centroiding, an annular mask collects detector pixels within the expected radius range. The laboratory calibration supplies

the mapping λ(θ), along with uncertainty, throughput, radial width, and PSF asymmetry as functions of wavelength and field angle. A reduced spectrum is formed by assigning a wavelength to each masked pixel and averaging radially, with corrections for detector response, source spectrum of the calibration system, and atmospheric transmission when used on sky.

A practical feature of this architecture is that the metasurface is passive. The design supplied for the current development effort uses a substrate diameter on the order of 600 um and a mass below one gram for the bench component. With appropriate packaging, the device can be placed in a filter-wheel or shutter location so that a telescope can switch between conventional imaging and Spectral Doughnut sensing. This dual-mode concept supports cueing: a conventional image can maintain star field awareness and track changes, while the metasurface mode can be inserted when a spectral measurement is needed.

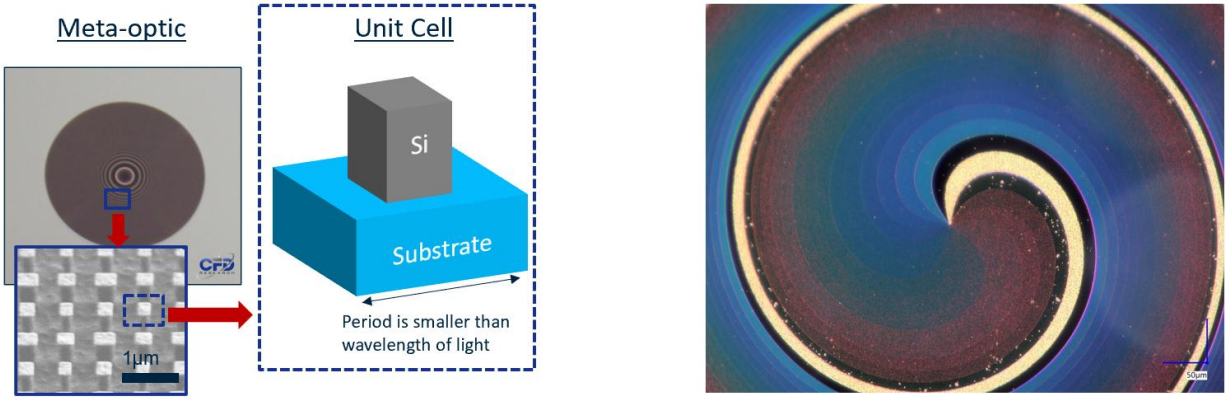


Figure 2 ***Metasurface operating principle. Subwavelength unit cells tune phase through geometry and material selection (Left) [15]. A chiral phase-gradient pattern creates a wavelength-dependent annular PSF (right).***

4 Optical Configuration

The Phase 1 demonstrator is designed around a commercially available 10-in f/8 Ritchey-Chretien telescope. The telescope provides a 250 mm aperture and 2000 mm focal length, uses a fully reflective primary/secondary configuration, and is therefore attractive for broadband work because it avoids primary chromatic aberration in the telescope itself. Manufacturer data list a 0.46 arcsec Dawes limit, 15.7 limiting magnitude, and a 35.3 lb optical-tube mass [8]. The telescope selection is pragmatic: it provides a low-cost path to on-sky testing and a familiar interface for alignment, tracking, and detector integration.

The present metasurface is placed in the converging beam near the telescope focus with a correction optic to compensate added optical power. This choice supports a compact proof-of-concept because it resembles a filter insertion location rather than a full spectrograph relay. It also creates a more difficult design problem than a pupil-plane implementation: rays incident on the metasurface vary with field position, pupil coordinate, and convergence angle. The Phase 1 configuration therefore emphasizes on-axis testing. A future full-field implementation would ideally place the metasurface at a conjugate of the entrance pupil, where the amplitude distribution and chief-ray geometry are better controlled across field angle.

The filter-wheel use case remains important even if the final full-field design uses an additional relay. A space- or ground-based surveillance telescope could operate in a conventional imaging mode for detection and tracking and then insert the metasurface for spectral characterization. The raw image would contain annular PSFs, but the telemetry product could be reduced spectra and centroids rather than full hyperspectral cubes, reducing the downstream data volume for sparse scenes.

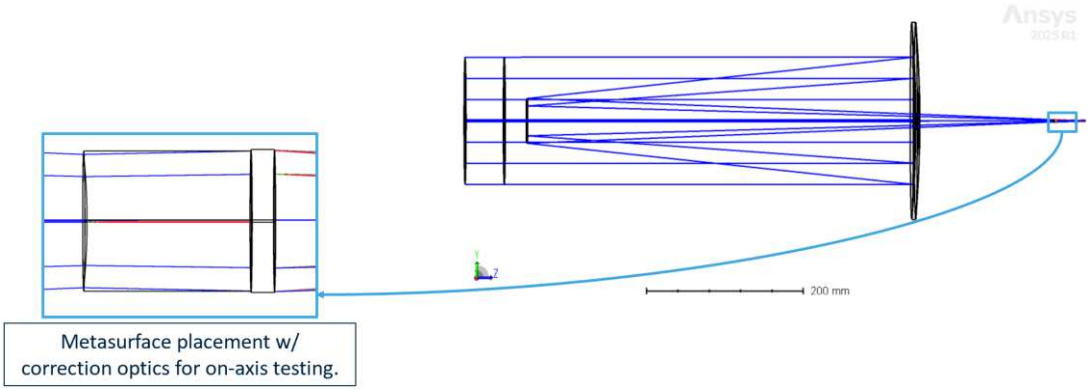


Figure 3. Current on-axis telescope integration concept. The metasurface and correction optics are inserted near the converging beam for a low-cost proof-of-concept. A pupil-conjugate placement is identified as the preferred future architecture for full-field operation.

5 Benchtop Calibration Plan

The calibration objective is to measure the wavelength-dependent PSF to determine the spectral resolution, throughput, alignment sensitivity, and repeatability of the fabricated metasurfaces. The benchtop setup uses a broadband quartz-tungsten-halogen (QTH) source, achromatic input optics, a Newport CS260B monochromator, achromatic relay optics, the metasurface assembly, and a cooled SWIR detector. A reference detector or spectrometer is used to characterize the source and monochromator before the metasurface is inserted. The planned detector is a WiDy SenS 640-class InGaAs camera, which provides 640 x 512 pixels, 17 µm pitch, and a 0.9-1.7 µm spectral response [9].

The alignment plan separates low- and high-sensitivity portions of the bench. Source, input, and collimating optics are aligned on an 8 ft by 4 ft optical bench. The emulator lens, aperture, metasurface, correction optic, and camera are aligned in a cage-mount system to improve axial repeatability. The same cage-based subsystem can then be adapted to the Orion telescope focus tube, reducing the risk of re-alignment between laboratory and on-sky tests.

The spectral reference measurement is performed before installing the metasurface. The camera position is replaced by an Ocean Optics NIR spectrometer or equivalent calibrated spectrometer, and the monochromator is stepped at 1 nm increments from 1.0 to 1.8 µm. This establishes the source/monochromator spectral response over a band wider than the 1.1-1.7 µm Spectral Doughnut design band. The result is used to correct subsequent images for source spectrum, monochromator throughput, detector response, and order-selection effects.

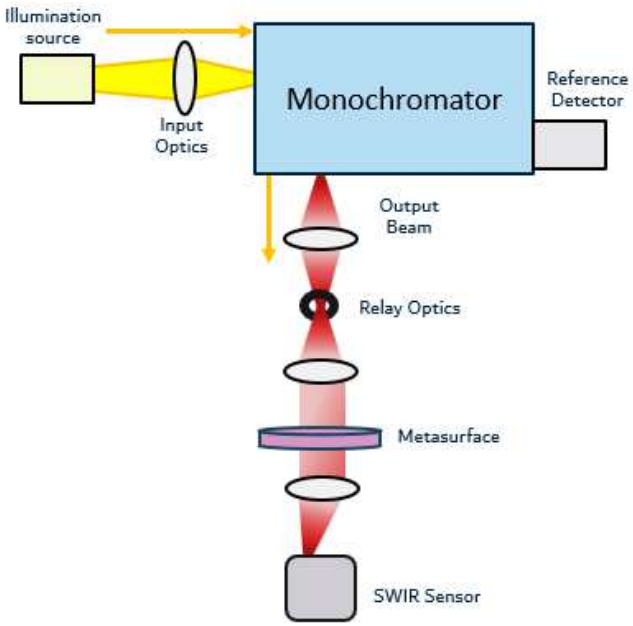


Figure 4. Benchtop calibration architecture. A broadband source is spectrally selected by a monochromator and relayed through the metasurface to a SWIR detector. A reference detector or spectrometer is used to calibrate source and monochromator response before and during the metasurface test.

Table 2. Calibration and validation sequence

Stage	Purpose	Nominal sequence
Reference spectral calibration	Measure source, monochromator, and relay response without the metasurface.	Replace camera with NIR spectrometer; step 1000-1800 nm in 1 nm increments.
Coarse metasurface calibration	Screen six metasurface elements and compare two manufacturing files before dicing.	Use whole wafer; step 1000-1800 nm in 40 nm increments; acquire dark and scene stacks.
Fine metasurface calibration	Create the wavelength-to-angle reference for the selected cut element.	Mount cut wafer behind correction optic; step 1080-1720 nm in 20 nm increments.
Snapshot line-lamp check	Verify calibration with known spectral lines and multi-wavelength scenes.	Acquire Hg, Ne, or Ar lamps after the monochromator-derived calibration.
On-sky transfer	Check instrument behavior under atmosphere and telescope tracking.	Collect empty sky background, reference star, and target satellite sequence.

6 Data Acquisition and Reduction

Each calibration wavelength step uses paired dark and illuminated image sequences. At least 30 dark frames and 30 illuminated frames are recorded per wavelength setting. Camera parameters are held fixed during a calibration run with optimal parameters determined during course testing. The draft calibration plan specifies linear response mode, approximately 10 ms integration time, and temperature stabilization before acquisition. The dark stack supports background subtraction, and nonuniformity correction removes pixel-to-pixel detector response variation before spectral extraction.

The image formation model for a sparse point-source scene can be seen below in 2): $\mathbf{I(x,y) = \Sigma_i \int S_i(\lambda) T(\lambda) h_\lambda(x-x_i,y-y_i)\, d\lambda + B(x,y) + n(x,y)}$. Here S_i(λ) is the source spectrum, T(λ) is system transmission, hλ is the wavelength-dependent Spectral Doughnut PSF, B is background, and n is detector and photon noise. The calibration problem is to estimate h_λ, T(λ), and the mapping λ(θ) with enough precision that $S_i(\lambda)$ can be recovered for each source.

2): $I(x,y) = \Sigma_i \int S_i(\lambda)\, T(\lambda)\, h_\lambda(x-x_i, y-y_i)\, d\lambda + B(x,y) + n(x,y)$

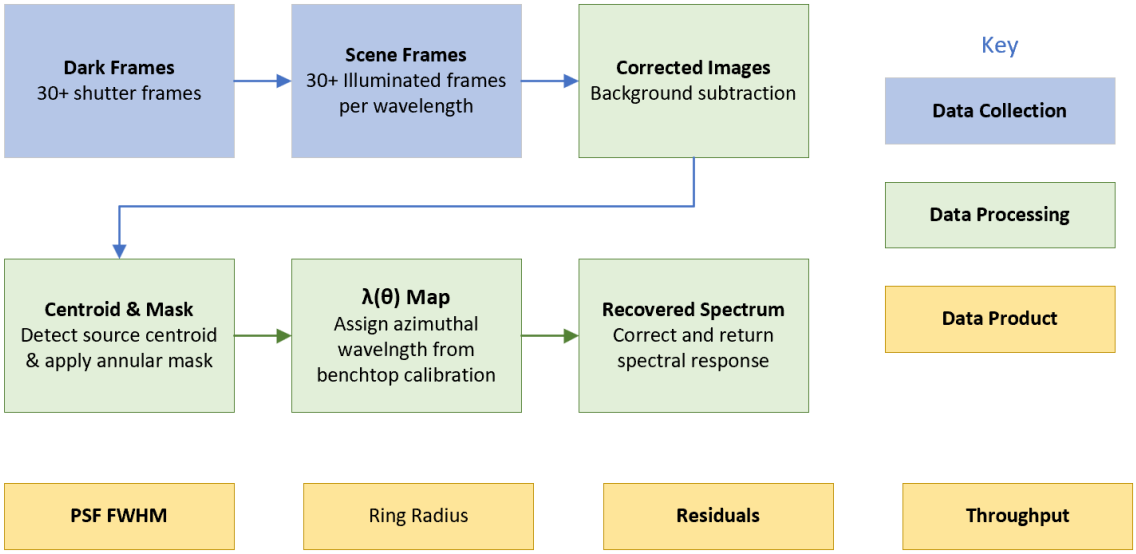


Figure 5. Reduction pipeline for calibration and data products.

The extraction algorithm is intentionally simple in the first implementation. A centroid is estimated for each PSF. With the ring radius known from calibration, an annular mask selects candidate spectral pixels. The lab-measured $\lambda(\theta)$ equation assigns wavelength to each pixel. Signal is averaged radially within angular bins to form a one-dimensional spectrum. Pixels affected by cosmic rays, bad-pixel maps, saturated glints, or overlap with neighboring rings can be excluded or given lower weight. This processing chain is well matched to sparse scenes and should be extended with a model-based multi-source fit for dense fields or ring intersections.

The calibration data products therefore include the measured residuals of the $\lambda(\theta)$ fit, radial PSF width as a function of wavelength, encircled energy, efficiency relative to the reference detector, centroid repeatability, spectral resolution measured from line sources, and cross-talk for simulated close pairs. These quantities are more informative than a single modeled spectral resolution number because the operational value of the architecture depends on calibration stability and extraction repeatability.

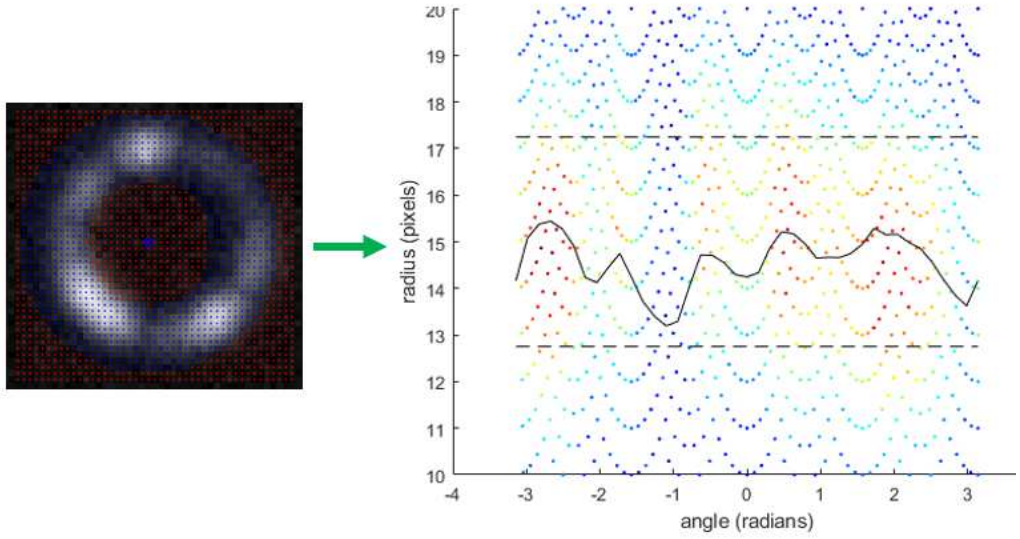


Figure 6. Representative annular extraction concept from the supplied simulations. Pixels are associated with angle and radius relative to the centroid, then radially averaged to generate spectral intensity as a function of angle and wavelength.

7 Modeled Phase 1 Performance

The current SWIR system was modelled as a diffraction element and imported to Zemax where the wavelengths can be varied within the 1.1-1.7 µm design band. Huygens PSFs were generated for discrete wavelengths and exported individually or combined into broadband simulations. The modeled wavelength-dependent PSFs can also be output as bitmap or numerical arrays for additional processing, allowing simulated source spectra to be weighted by the proportional wavelength response of the Spectral Doughnut PSF.

Figure 7 shows representative monochromatic PSFs across the design band. The simulations demonstrate the intended wavelength-dependent azimuthal rotation of the annular PSF, where the dominant energy distribution rotates around the ring as wavelength changes. This rotational behavior forms the basis for spectral reconstruction using calibrated angular position around the source centroid. The modeled PSFs also show higher-order diffraction structure and fringing artifacts, particularly at larger radii and longer wavelengths. These effects are expected in an early metasurface implementation and indicate areas for future optimization and calibration refinement.

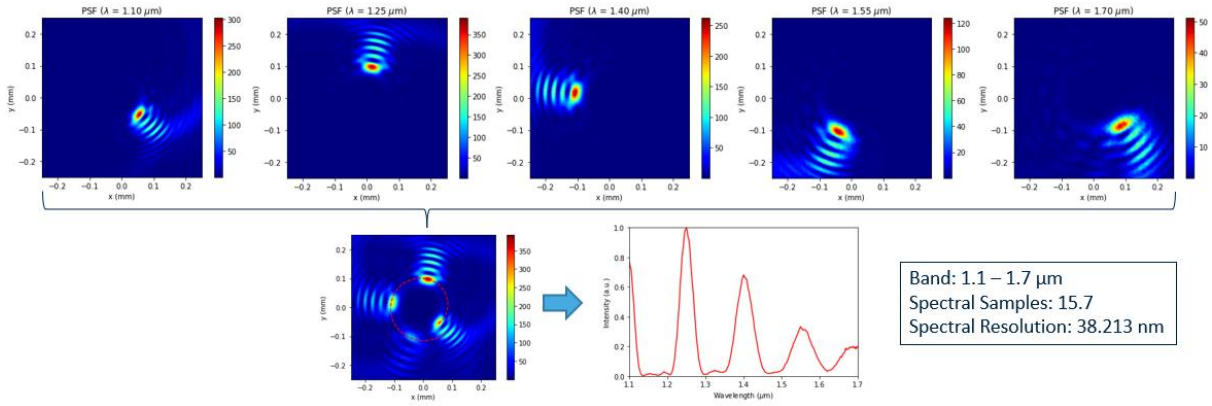


Figure 7. Initial modeled SWIR PSF sequence and spectral response from the Phase 1 design.

The Zemax outputs were also used to create broadband simulations by combining individual wavelength PSFs using weighted source spectra. Figure 8 shows a representative broadband simulation using a 3200 K quartz–tungsten–halogen (QTH) spectral weighting function. The resulting composite Spectral Doughnut PSF demonstrates how broadband energy redistributes around the annular structure as a function of source spectrum and detector response. The associated central cross section highlights the spatial-frequency structure of the combined response.

These initial simulations were used to investigate potential low-compute extraction methods, including annular averaging and transform-based approaches such as Radon transforms, while also providing insight into alignment sensitivities, wavelength sampling density, and PSF overlap behavior. The modeled wavelength-dependent rotation of the annular PSF remained observable across the design band, although higher-order diffraction structure and fringing artifacts were also present in the simulated response. These effects are expected in early metasurface implementations and will require calibration and future optimization to improve spectral separation and reconstruction. The present results summarized in Table 3 remain simulation-based and require laboratory validation using monochromator measurements and spectral line sources before system performance can be experimentally verified.

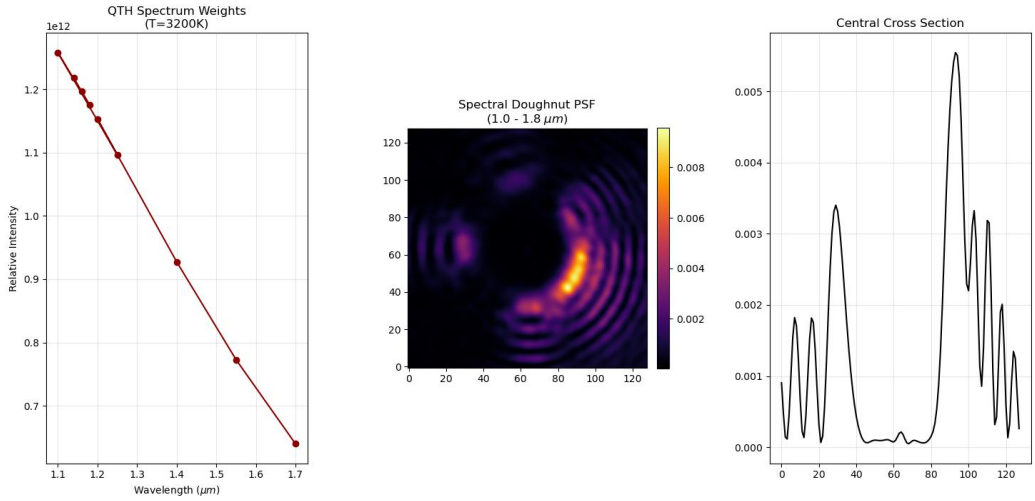


Figure 8. ***Representative numerical simulation of a broadband source passed through the Spectral Doughnut PSF.***

Table 3. Phase 1 design values and interpretation.

Parameter	Phase 1 value or target	Interpretation
Spectral band	1.1-1.7 µm	SWIR proof-of-concept band.
Modeled spectral resolution	38.213 nm	Modeled value pending monochromator and line-lamp validation.
Spectral samples	15.7 across band	Computed from 600 nm bandwidth divided by modeled resolution.
Resolving power	R about 37 at 1.4 µm	Moderate resolution; not intended as high-resolution spectroscopy.

8 On-sky Demonstration Strategy

The on-sky campaign is intended to transfer the laboratory calibration into a telescope observation with environmental effects. The plan is to integrate the cage-mounted metasurface/correction-optic assembly with the Orion focus tube, block stray light, and verify alignment using the same optical references used on

the bench. The observation sequence should include three acquisitions: a shutter image for background subtraction, a reference star for atmospheric and instrument response, and the target satellite or RSO. A co-boresighted telescope and satellite-tracking software can provide initial pointing and acquisition for LEO passes.

The reference star observation is critical. Ground-based SWIR spectra are affected by telluric absorption, air mass, sky background, and time-varying sources. A reference star near the target track and time provides the information needed to correct atmospheric throughput and to check the $\lambda(\theta)$ calibration after the instrument is mounted on the telescope. If the target spectrum is used for material inference, uncertainty should include reference-star selection, air-mass mismatch, scintillation, and integration-time differences.

A useful first on-sky success criterion would not be classification of a specific spacecraft. A more defensible sequence is:

1. Demonstrate that a star produces the calibrated ring at the expected radius and angle
2. Recover a repeatable broad-band spectrum for stars of different color temperature
3. Recover a spectrum for a bright satellite pass
4. Compare the recovered satellite spectrum with simultaneous or near-simultaneous conventional radiometry or a reference spectrometer.

Table 4. Technical risks and planned mitigations.

Risk or limitation	Why it matters	Mitigation or measurement
On-axis demonstrator only	The current converging-beam layout does not fully validate wide-field performance.	Design future pupil-conjugate relay and measure field dependence.
Fringing and higher-order PSF structure	Can bias radial averaging and reduce effective spectral resolution.	Report PSF residuals
Atmospheric transmission	Ground-based SWIR response varies by wavelength and time.	Observe reference stars and include a telluric correction uncertainty.
Ring overlap in dense scenes	Closely spaced sources can still intersect in two locations.	Mask intersections or fit multiple calibrated PSFs jointly.
Detector nonlinearity and bad pixels	Spectral features can be confused with response artifacts.	Use linear mode, dark stacks, NUC, and bad-pixel maps
Fabrication variability	Subwavelength features are sensitive to process tolerances.	Screen multiple elements; compare two manufacturing files; report throughput and calibration scatter.

9 Discussion

The Spectral Doughnut metasurface concept proposed and demonstrated through design and simulation presents a mission-specific hyperspectral cueing architecture for unresolved point sources, making it well suited for mapping resident space objects (RSOs). This distinctive wavelength-dependent point spread function (PSF) redistributes spectral information azimuthally around a point source rather than dispersing it along a linear axis. As a result, optical energy remains more localized to the source centroid, enabling improved centroiding performance, enhanced spatial positioning accuracy, and reduced axial spectral smearing. The approach addresses a notable gap in spectroscopy for sparse astronomical scenes while providing a comparatively simple implementation through the use of a metasurface-based optical element.

The Phase I concept demonstrates promising performance, achieving an R value of 37, which may be traded against bandwidth and wavelength range requirements and potentially improved through additional phase optimization and refinement of spectral extraction techniques. Although the architecture is not intended to replace high-resolution spectroscopy, the filter-based method provides supplementary spectral content that increases confidence in system-level object characterization and supports continued monitoring of stars and RSOs when combined with additional measurements and observational data.

The present work establishes a proof-of-concept pathway for modeling, calibration, and on-axis telescope integration; however, several limitations remain. The current converging-beam implementation does not fully validate the wide-field behavior implied by the concept because the metasurface experiences varying incidence angles and pupil geometries across the field. To resolve this a future pupil-conjugate implementation will be necessary to evaluate wide-field stability, off-axis spectral reconstruction performance, and field-dependent calibration behavior. Depending on the final optical architecture, achieving full-field operation may require additional relay optics, potentially reducing some of the compact filter-wheel advantages demonstrated in the present configuration.

Simulations additionally indicate that the wavelength-dependent annular response is accompanied by higher-order diffraction structure and fringing artifacts, which may broaden the effective spectral response and increase sensitivity to alignment and fabrication tolerances. Benchtop validation using monochromator measurements and calibrated spectral line sources will therefore be required before modeled performance metrics can be considered experimentally verified. Within these limitations, the current SWIR design is intended for moderate-resolution spectral sensing focused on broad material-class discrimination, spectral cueing, and anomaly detection rather than high-dispersion spectroscopy. The operational value of the architecture lies primarily in its compact passive implementation, snapshot acquisition capability, reduced spectral overlap in sparse scenes, and compatibility with existing telescope systems.

10 Future Work

The next development phase is planned and proposed to close four gaps as follows. First, the fabricated metasurface elements must be calibrated against the monochromator and line lamps to replace modeled values with measured spectral resolution, throughput, and uncertainty. Second, the extraction algorithm should advance utilizing the captured benchtop test data developing a spectral wrapping function, account for field-dependent aberrations, and realistic detector noise. Third, the optical design should move the metasurface to a conjugate plane of the entrance pupil to enable the full-field claim. Fourth, additional bands should be pursued only after the SWIR validation demonstrates repeatable performance.

The visible-band design path is compelling because a 400-1000 nm band with 10 nm spectral resolution would align with many astronomical detectors and material-classification use cases as well as improving the diffraction limited performance of the system. Extension to MWIR and LWIR may also be possible in principle, but it will require different materials, detector technologies, and thermal-background models resulting in new fabrication constraints. Spectropolarimetry is another logical follow-on because metasurfaces can be designed to encode polarization as well as wavelength, potentially enabling simultaneous spectral and polarization cues for object characterization.

The most valuable next data products are a concise set of validation plots: measured $\lambda(\theta)$ with residuals, spectral-line response and FWHM across the band, throughput versus wavelength, field-dependent PSF stability, close-source cross-talk tests, and an on-sky demonstration on a star and a bright LEO object. These results will convert the present design study into an experimental validation of the architecture.

11 Conclusions

Spectral Doughnut is a metasurface enabled approach to snapshot spectral sensing of unresolved point sources. By engineering a wavelength-dependent chiral PSF, the architecture preserves centroid information while mapping spectra azimuthally around each source. This geometry is well suited to sparse

astronomical scenes and can reduce the axial spectral mixing that affects conventional slitless spectrometers when objects are closely spaced along the dispersion direction.

The Phase 1 SWIR design targets a 1.1-1.7 μm band with modeled 38.213 nm spectral resolution and approximately 15.7 spectral samples. The proof-of-concept uses a compact metasurface and correction optic in an f/8 Ritchey-Chretien telescope path and a benchtop monochromator calibration with a cooled InGaAs focal plane. The benchtop calibration sequence, data-reduction pipeline, and on-sky plan are prepared, but measured laboratory and telescope results are required before strong performance claims are made.

With those results, Spectral Doughnut can be positioned as a low-SWaP-C spectral augmentation for SDA telescopes rather than as a general-purpose high-resolution spectrograph. The next validation steps are to distinguish current on-axis behavior, replace modeled values with measured values, report uncertainty, and complete the tolerance analysis needed for reproducible calibration and analysis.

Declarations and data availability

Conflict of interest: Authors Lukas Senczyszyn, Christian Conkle, and Zachary Coppens are named inventors on a pending patent application related to the Spectral Doughnut metasurface-based hyperspectral imaging architecture and/or associated data-processing methods. The patent application is jointly owned by Space Dynamics Laboratory/ CFD. The authors declare no other competing financial or non-financial interests relevant to the content of this article.

Data availability: The results presented in this article are based primarily on optical modeling, system design analysis, and planned laboratory calibration procedures for the Spectral Doughnut prototype. No public dataset repository has been established at the time of submission. Because a patent application related to the Spectral Doughnut metasurface architecture and/or associated data-reduction approach has been filed, detailed metasurface design files, fabrication files, and other enabling technical data are not publicly available. Non-proprietary modeling outputs and processed data supporting the figures in this article may be made available from the corresponding author upon reasonable request, subject to institutional approval and applicable intellectual-property, sponsor, export-control, or nondisclosure restrictions.

References

[1] Vasile, M., Walker, L., Dunphy, R. D., Zabalza, J., Murray, P., Marshall, S., and Savitski, V., Intelligent characterisation of space objects with hyperspectral imaging, Acta Astronautica, 203, 510-534, 2023. https://doi.org/10.1016/j.actaastro.2022.11.039.

[2] Vasile, M., Walker, L., Campbell, A., et al., Space object identification and classification from hyperspectral material analysis, Scientific Reports, 14, Article 1570, 2024. https://doi.org/10.1038/s41598-024-51659-7.

[3] Velez-Reyes, M., Najera, A., Porras, L., DeBlasio, D., and Erives, H., Understanding spectro-temporal signature variability of unresolved resident space objects using a simulation model, Advanced Maui Optical and Space Surveillance Technologies Conference, 2023.

[4] Newport, The Grating Equation, MKS/Newport technical note, accessed 16 May 2026.

[5] Edmund Optics, All About Diffraction Gratings, Edmund Optics Knowledge Center, accessed 16 May 2026.

[6] Hu, X., Xu, W., Fan, Q., Yue, T., Yan, F., Lu, Y., and Xu, T., Metasurface-based computational imaging: a review, Advanced Photonics, 6(1), 014002, 2024. https://doi.org/10.1117/1.AP.6.1.014002.

[7] Lin, C.-H., Huang, S.-H., Lin, T.-H., and Wu, P. C., Metasurface-empowered snapshot hyperspectral imaging with convex/deep (CODE) small-data learning theory, Nature Communications, 14, Article 6979, 2023. https://doi.org/10.1038/s41467-023-42381-5.

[8] OPT Telescopes, Orion 10 in f/8 Ritchey Chretien Reflecting OTA Telescope specifications, accessed 16 May 2026.

[9] New Imaging Technologies, WiDy SenS 640 high sensitivity and HDR SWIR camera specifications, accessed 16 May 2026.

[10] Ding, K., Wang, M., Chen, M., Wang, X., Ni, K., Zhou, Q., and Bai, B., Snapshot spectral imaging: from spatial-spectral mapping to metasurface-based imaging, Nanophotonics, 13(8), 1303-1330, 2024. https://doi.org/10.1515/nanoph-2023-0867.

[11] Eismann, M. T., Hyperspectral Remote Sensing, SPIE Press, Bellingham, WA, 2012.

[12] Goodman, J. W., Introduction to Fourier Optics, 4th ed., W. H. Freeman, New York, 2017.

[13] Space Telescope Science Institute (STScI), "JWST Wide Field Slitless Spectroscopy," JWST Documentation, accessed 26 May 2026. Available: https://jwst-docs.stsci.edu/methods-and-roadmaps/jwst-wide-field-slitless-spectroscopy#gsc.tab=0.

[14] Space Telescope Science Institute (STScI), "NIRCam Wide Field Slitless Spectroscopy," JWST Documentation, accessed 26 May 2026. Available: https://jwst-docs.stsci.edu/jwst-near-infrared-camera/nircam-observing-modes/nircam-wide-field-slitless-spectroscopy#gsc.tab=0.

[15] Wirth-Singh, A., Fröch, J. E., Han, Z., Huang, L., Mukherjee, S., Zhou, Z., Coppens, Z., Böhringer, K. F., and Majumdar, A., "Large field-of-view thermal imaging via all-silicon meta-optics," Applied Optics, 62(20), 5467–5474, 2023. https://doi.org/10.1364/AO.486025.